Construction and Building Materials 231 (2020) 117086

Contents lists available at ScienceDirect

Construction and Building Materials

journal homepage: www.elsevier.com/locate/conbuildmat

Assessment of damage distribution in brittle materials by application of an improved algorithm for three-dimensional localization of acoustic emission sources with P-wave velocity calculation

Patricia Rodríguez [a,*], Tarcisio B. Celestino [b,c]

[a] Ferrara Proyectos Especiales, Santiago 7770112, Chile
[b] Department of Geotechnical Engineering, São Carlos Engineering School, University of São Paulo, São Carlos, SP 13566-590, Brazil
[c] Themag Engenharia Ltda., São Paulo, Brazil

HIGHLIGHTS

- An improved algorithm is applied for localization of AE sources with v_p calculation.
- CLAPWaVe algorithm is applied to assess the damage distribution in rock specimens.
- v_p values distribution provide information related to evolution of damage in rocks.
- A non-homogeneous distribution of damage inside the rock specimens was observed.
- Using a unique value for v_p for localization may lead to unrealistic analyses.

ARTICLE INFO

Article history:
Received 21 June 2019
Received in revised form 23 September 2019
Accepted 25 September 2019
Available online 19 December 2019

Keywords:
Three-dimensional localization
Acoustic emission
Damage distribution
P-wave velocity distribution
v_p values evolution
CLAPWaVe

ABSTRACT

An improved algorithm for acoustic emission source localization with P-wave velocity v_p calculation and an enhanced methodology for P-wave onset time determination, called CLAPWaVe [1], is applied to analyze the distribution of damage within rock specimens under diametral compression. The analyses allowed the identification of four zones of damage accumulation within the specimen volume, each of them with different cracking levels, absolute energy release and associated v_p values. The observed non-homogeneous damage distribution confirms that using a unique v_p value for the localization of all AE sources, as usually adopted, is not representative of the real condition of the specimen.

1. Introduction

The tensile stresses generated by local stress concentration at microscopic flaw scale inside quasi-brittle materials are responsible for the initiation and development of their rupture process. The determination of cracking patterns inside the specimens of brittle materials is not yet well understood; such characterization should be done by using real brittle specimens (rock or rocklike).

The crack propagation process inside brittle materials releases energy as elastic waves, known as acoustic emission (AE) [2]. The AE monitoring is a non-destructive technique that enables the complete observation of the cracking process inside the volume of the specimen during all the test, without inducing any disturbances [2–4]. Given the characteristics of the initiation of the damage process, experimental analysis of specimens subjected to tensile stresses, monitored with AE, is an adequate option to achieve real understanding of this process.

Monitoring of crack propagation has been carried out by using different AE parameters (for example, AE energy, amplitude, raise time, average frequency, AE counts, AE events) together with b-value analysis [5,6]. However, such research works have not included spatial analyses of the cracking pattern inside of the specimens by using three-dimensional localization of AE sources.

* Corresponding author.
E-mail addresses: patricia.rodriguez@ferrara.cl, pcrodris@uc.cl (P. Rodríguez), tbcelest@usp.br (T.B. Celestino).

https://doi.org/10.1016/j.conbuildmat.2019.117086
0950-0618/

The distribution of damage inside a specimen under loading can be obtained by the localization of AE sources. Localization of AE sources together with some AE parameters [7], with moment tensor analyses [8] or with b-value analyses [9] has been applied to assess the evolution of the damage process in concrete specimens. Complementary evaluations of the cracking process by including three-dimensional localization, AE parameters and b-value analyses has been applied to concrete specimens [10]. Three-dimensional localization algorithms proposed in the literature still need improvement. Several works have reported the three-dimensional localization of AE sources [2,11–16], but they consider v_p as a known value, that remains unchanged while damage is induced in the specimen. This assumption is not realistic and may affect the accuracy of the localization process and the accuracy of the AE sources pattern obtained. The v_p value calculation in the three-dimensional localization algorithm has been included in some research works [17–19], however, they used such information just for the adjustment of the localization process [17] or they adopt a separate group of sensors specifically for measuring v_p [18]. Li and Dong [19] proposed a solution for the three-dimensional localization of AE sources with v_p calculation, but their algorithm requires previously known information about the onset of signal to each sensor.

Improved cracking pattern analyses in brittle materials by using different cluster methodologies have been reported in the literature. [16,20–22]. Carpinteri [20] carried out b-value analysis to study the damage process inside concrete specimens subjected to compression. Those authors also correlated the b-value analyses with the fractal dimension D to characterize the spatial distribution of damage by means of AE monitoring. Rodríguez and Celestino [16] report on the cluster the AE sources by using their intensity levels measured as AE energy in rock specimens subjected to diametral compression tests. Iturrioz et al. [21] conducted b-value analyses [9] by dividing the test into different stages of loading (linear and deviations from linear behavior) to better assess the damage process in concrete specimens subjected to uniaxial compression tests and three-point bending tests. Manthei [22] analyzed the cracking process in a cylindrical rock salt specimen under tensile load by using the fractal dimension D of the events. Those authors conducted such analyses by defining time and distance clustering parameters [22].

Because both the P-wave arrival time and the v_p value are dominant factors involved in the accuracy of the three-dimensional localization of AE sources, an algorithm incorporating improvements for both aspects, called CLAPWaVe (Crack Location by Acoustic emission with P-Wave Velocity determination) [1], is applied in this manuscript. CLAPWaVe is an iterative three-dimensional localization algorithm, that includes a more efficient searching algorithm, an improved methodology for P-wave arrival time determination, independent of a predefined amplitude threshold, and calculates the coordinates of each AE source as well as the associated v_p value [1]. In addition, CLAPWaVe incorporates and improved visualization tool to obtain enhanced cracking patterns, based on the general tendency of each group of data (x, y, z, v_p). The clustering of the AE sources based on their intensity levels, i.e., on their levels of absolute energy released (E_A), is an appropriate way to highlight the main damaged areas in specimens under any loading condition [1]. A similar clustering tool was considered in Rodríguez and Celestino [16], but in this research the AE Energy was considered instead of E_A.

This manuscript reports on the application of CLAPWaVe for the characterization of the cracking process, the cracking pattern and evolution of integrity within two different types of rocks, marble and monzogranite, under monotonic displacement-controlled diametral compression tests. The characterization process is performed using complementary analyses of the pattern of localized AE sources, and the distribution of both v_p and E_A inside the specimen volume during the loading process.

2. Materials and methods

2.1. Test setup

A stiff servo-controlled testing system with maximum loading capacity of 2700 kN was used. The procedure suggested by Celestino et al. [23,24] was adopted to allow controlling the post-peak region of diametral compression tests. An eight-channel system and six wide band piezoelectric AE sensors, developed by Physical Acoustics South America (PASA), were used to monitor the cracking process (three on each face of the rock specimens). A dual averaging extensometer was used to control the displacement along the diameter perpendicular to the loading direction. Fig. 1 shows the typical test setup used for all the tests in both rocks.

For the purpose of result interpretation, besides the coordinates (x, y, z) of each AE source and their corresponding v_p value, a relevant AE parameter was calculated for each AE signal (henceforth called waveforms) used in the three-dimensional localization process, which is the absolute energy, E_A. The absolute energy (aJ) of a signal is calculated as the integral of the square of the voltage V(t) divided by the impedance of the AE system, R. Waveforms were recorded using AEwin® software from PASA [25], and the gain was set to 40 dB. The acquisition rate for waveforms collection was adjusted to 1 MHz.

2.2. Specimens

Disc-shaped rock specimens with 100 mm diameter and 50 mm thickness were subjected to displacement-controlled diametral compression tests. Two types of rock specimens were selected for this research: marble and monzogranite. Marble specimens were collected from the Italva Group, Brazil, and monzogranite specimens were collected from the Cantareira Batholith, Brazil. Both rocks exhibit macroscopic homogeneity in its intact condition, but different mechanical behavior and geological features. Marble is an essentially monomineralic metamorphic rock (calcite), that exhibits a high number of natural microcracks (cleavage planes). Monzogranite is a polymineralic igneous rock with an imbricated crystalline structure and low number of natural microcracks, without any preferential path for crack propagation [16]. Therefore, those rocks evolve in different cracking patterns, when they are subjected to loading. Such differences in behavior enable better visualization of the results provided by CLAPWaVe. The same concepts are applicable to other similar materials.

3. Theoretical concepts

Three-dimensional localization with CLAPWaVe includes both the calculation of coordinates of each AE source (x, y, z) and the corresponding v_p value [1]. The localization algorithm requires information of the coordinates of each sensor, i, located on the specimen surface and the relative arrival times of the P-wave at each sensor i, measured from the moment the trigger sensor receives the first signal. CLAPWaVe can perform the localization by using a network of at least five sensors distributed on the surface of the specimen, even better when six or more sensors are used.

Usually, the methods used for the localization of AE sources require definitions of v_p and the wave amplitude threshold value, which must be provided at the beginning of the test [1]. The v_p value imposed as an input value for the localization remains unchanged whether or not cracking has already initiated in the

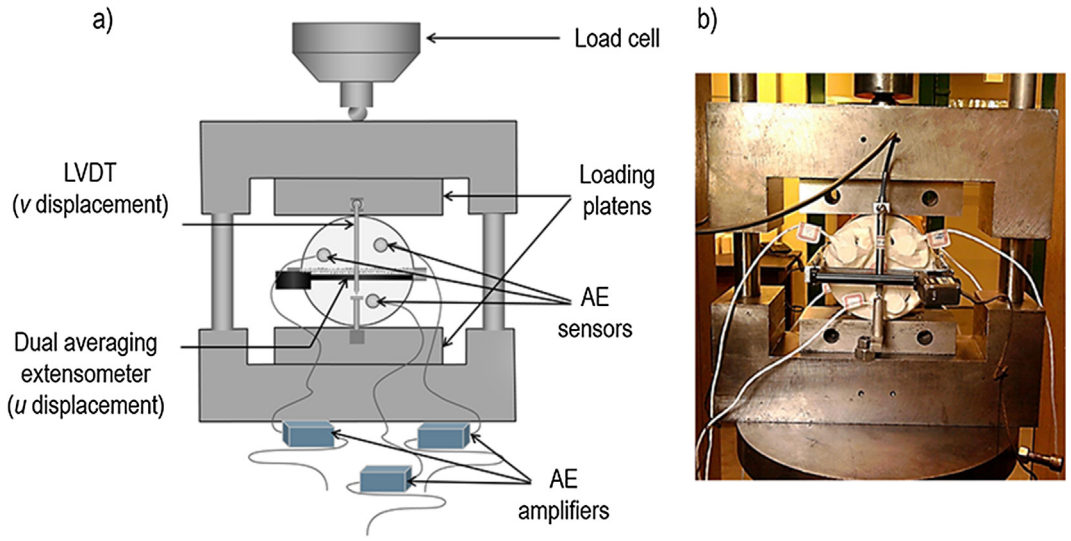

Fig. 1. Test setup and instrumentation for AE monitoring and displacement control of brittle failure under monotonic diametral compression test. a) Schematic setup. b) Typical setup.

specimen. Different from other typical localization algorithms, CLAPWaVe determinates v_p together with the coordinates for each AE source along the time, therefore, four unknown variables are calculated and at least five sensors are required for localization with v_p determination. In addition, CLAPWaVe adopts an appropriate methodology for the determination of the P-wave arrival time (henceforth called AIC-TC1.1) independent of a predefined wave amplitude threshold. Typical search methodologies included in localization algorithms only work by evaluating the objective function at different points so as to find the minimum, i.e., the Simplex algorithm [26,27]. The search algorithm applied in CLAPWaVe include the introduction of a gradient for the fast definition of the optimum search direction.

AIC-TC1.1 includes concepts of the AR-AIC method [28,29] to define the noise segment of the signal without the previous definition of a wave amplitude threshold. A variable amplitude threshold based on the characteristic of the noise segment of each specific waveform is estimated, by using the concepts proposed in the TC method [30]. The AIC-TC1.1 method searches for the first peak in intensity of the waveform, higher than the noise level. In comparison with the Autoregressive Akaike Information Criterion (AR-AIC) method, the Threshold Crossing (TC) method and the First Threshold Crossing (FTC) method [29,31], the proposed methodology for detection of the P-wave arrival time has shown to be the more accurate for applications of AE source localization and determination of P-wave velocity.

Current methodologies for three-dimensional AE source localization include: i) the Simplex search algorithm which requires the definition of a threshold value; ii) the First Threshold Crossing (FTC) method for P-wave arrival time detection; and iii) the v_p value as a constant value, defined at the beginning of the test. The accuracy of localization of the before mentioned algorithms was compared with CLAPWaVe. It was observed that the mean error of localization obtained with the former methods was of the order of 10^{-7} s, while with CLAPWaVe, such value was reduced to about 10^{-19} s.

For the purpose of analyses, the P-wave velocity of the intact specimen v_{p_in} is obtained before the test. Such value is estimated by inducing artificial AE sources based on pencil lead breaking [32]. The wave trajectories considered for v_{p_in} should include one sensor on each face of the specimen in order to guarantee wave propagation across the specimen volume.

Because the localization process searches for four unknown variables (x, y, z, v_p), such v_p value characterizes the mean properties of the specimen volume, defined along the trajectories between the AE source and each of the AE sensors that receive the signal emitted by this AE source. Therefore, the trend of the average v_p values, associated to each AE source allows the analysis of the distribution and evolution of damage, strength and stiffness inside the volume of the specimen during the loading process.

4. Results and discussion

4.1. Typical behavior in monzogranite under diametral compression tests

Fig. 2 shows the cumulative spatial distribution of AE sources and their corresponding v_p values, from the beginning of the test up to each loading stage. Fig. 2 displays seven control points, 1 to 7, representing loading stages, at which the location of AE sources and corresponding v_p values are presented (see load-time relationship at the bottom-center of the figure). The control points 1 to 3 are located at 50, 75, and 100% of the peak load, respectively. The control points 4 to 7 are typical of different post peak stages of loading, including the end of the test. The different ranges of v_p values inside of the specimen are represented by a color scale, which is shown at the bottom left of the figure. The size of the dots, shown in images 1 to 3 of Fig. 2, was increased to enable a better visualization of the pattern at the first loading stages, where only a few AE sources were localized. At the end of the test (Image 7), the large number of localized AE sources might hinder a complete visualization of the pattern of v_p values in the XY plane. For the sake of clarity, a lateral view at the same stage (YZ plane) is shown at the middle right of the figure.

Image 1 of Fig. 2 shows only two localized AE sources at the region of contact between the specimen and the loading platens. Their location and the low levels of E_A released at this stage, as further discussed later, suggest that they are not related to the initiation of microcracking, but to the process of adjustment between loading platens and specimen during initial loading stages.

From control point 2 onwards, AE sources with v_p values lower than that of the intact condition (v_{p_in} = 4659 m/s) accumulate at the center of the specimen. Their v_p values and the higher levels of E_A released (see Fig. 4h) suggest that they are associated with

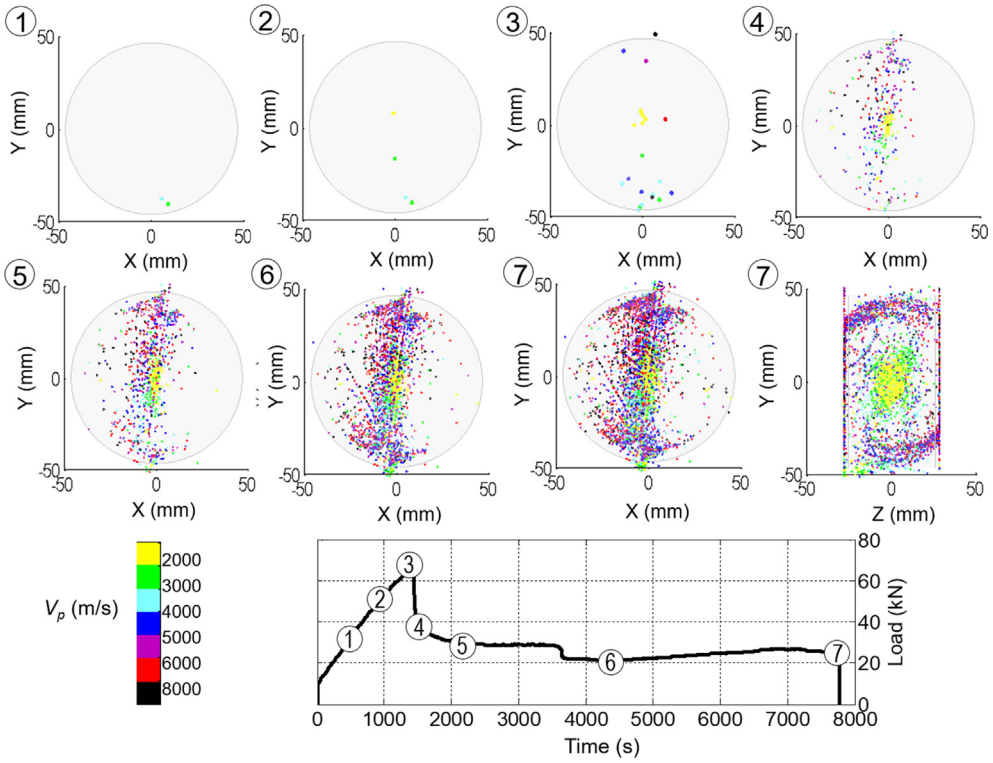

Fig. 2. Typical cumulative spatial distribution of AE sources and their corresponding v_p values, from the beginning of the test up to each loading stage during monotonic displacement diametral compression test on a monzogranite specimen (results obtained by application of CLAPWaVe).

the initiation and propagation of microcracking. The load dropping stage after peak (from control point 3 to 4 in Fig. 2) is quite short. Natural microcracks in the material are quite small and not necessarily are they favorably oriented for propagation, with respect to the maximum tensile stresses on the diameter parallel to the loading direction. The test can be stable if the load is controlled according to the rule of constant diametral displacement along the diameter perpendicular to the loading direction [23,24]. When the peak is reached, the crack opens, significantly increasing the diametral displacement. At the final stages of the test, the load even increases as the crack reaches the confined region affected by the contact with the loading platens. Images 2 to 7 of Fig. 2 show that, during the test, a central damage core is generated. Such zone concentrates AE sources with v_p values much lower than that of the intact condition, and lower than any other zone of the specimen. Images 7 (planes XY and YZ) show the clear damaged core zone, while the region of contact between the specimen and the loading platens shows v_p values similar and even higher than that of the intact condition. Also, the region close to the faces of the specimen shows v_p values that oscillate around that of the intact condition.

The presence of AE sources with v_p values lower, similar and higher than that of the intact condition (v_{p_in} = 4659 m/s) suggest that, more than one effect acts at this contact zone that generates AE sources: 1) The transference process between the specimen and the loading platens can create some AE sources, which are associated to the noise produced at the contact zone, because of the small irregularities at the surface of contact between the specimen and the loading platens; 2) The confinement induced by the loading platens to the specimen at the vicinity of the contact zone produces AE waves that travel from the source to the sensors through a confined region, exhibiting associated v_p values higher than that of the intact condition. The theoretical expressions [33,34] and the numerical simulations [35], both performed considering specimens of homogeneous materials subjected to diametral compression, showed that stresses along the X-axis are compressive close to the region of contact between the specimen and the loading platens. Also, in diametral compression tests, when a compressive load is applied along the Y-axis of the specimen, the higher stiffness of the loading platens, in comparison with the rock specimen, induces compressive stresses along the Z-axis in the region of contact between both materials. Therefore, a three-dimensional confinement effect develops in that region, which increases with loading. The confinement increases the stiffness of the specimen in this zone, which in turn reduces the time of traveling of AE waves through that region, producing v_p values similar to or even higher than those of the intact specimen condition, even when that zone has been damaged. 3) Local failure of the less confined region of the contact zone, which occurs at later stages of the test. At those stages of the test, the central core of the specimen concentrates tensile stresses, resulting in more damaged zone, and producing stress redistribution inside of the specimen. Along the loading axis, the central core is the most damaged zone and the contact zone is less damaged. The less damaged regions located along the loading axis receive the higher portion of the load, which could lead to the local failure of the specimen at the external region of the contact zone, where the influence of confinement by the loading platens to the specimen is lower. The AE sources associated to the effect 3 are generated at the less confined contact zone, and the waves travel through a less confined region with different levels of damage. Therefore, the travel times between the source and the sensors increase and the v_p values decrease.

In images 1 to 2 of Fig. 2, the AE sources localized at the contact region, with v_p values lower or equal to that of the intact condition, suggest predominance of effect 1 beforementioned. Image 3 of Fig. 2 shows the initiation of the effect 2, and at Image 4 that effect has been clearly defined (v_p values higher than that of the intact condition). From that point on, effect 2 is still predominant, but between control points 5 and 6, the accumulation of AE sources at the lower contact zone, with associated v_p values lower than

that of the intact condition, are observed (yellow, cyan and green dots). The location of those AE sources, at the edge of the bottom contact zone, and their v_p values suggest that they are associated to the effect 3.

The localized AE sources and the distribution of v_p values, shown in images 1 to 7 of Fig. 2, clearly show that cracking initiates at the central core of the specimen, in consistence with the expected damage pattern in this type of tests [36]. Fig. 2 also shows that the damage is not homogenously distributed inside of the specimen volume.

Fig. 3 shows the final cracked specimen. The faces of the specimen are identified by the number of the sensors placed on them. Thus, on face 123, the AE sensors identified by the numbers 1, 2 and 3 were placed. The same is valid for the face 456. For a better visualization of the cracked area of the specimen, Fig. 3 shows detailed pictures where the central areas of the specimen are enlarged. To improve the visualization of the damaged area in the specimen, a thin layer of white chalk dust was used to cover the cracked region, resulting in better contrast between the cracked and intact areas.

Complementary analyses were performed by clustering the AE sources based on their levels of absolute energy E_A. The cumulative spatial distribution of AE sources corresponding to each of the seven control points shown in Fig. 3, highlighted by cluster boxes representing accumulated E_A, were obtained with the localization data provided by CLAPWaVe. Such analyses enabled a better visualization of the cracking pattern inside the volume of the specimen by highlighting the main damaged areas [1]. By performing analyses of the v_p values together with the beforementioned assessment of the pattern of AE sources clustered by the E_A of each AE source, four zones of damage accumulation with different characteristics were identified: contact region (blue sources, Fig. 4a), internal core (red sources, Fig. 4b), external core (green sources, Fig. 4c) and boundary zone (pink sources, Fig. 4d). The contact zone contains the AE sources located close to the region of contact between the specimen and the loading platens; the internal core contains the AE sources located in a close vicinity of the center of the specimen, and the external core contains those located in the central region of the specimen, but close to its faces. Those three zones are located along the loading axis, defining the typical failure surface observed in diametral compression tests.

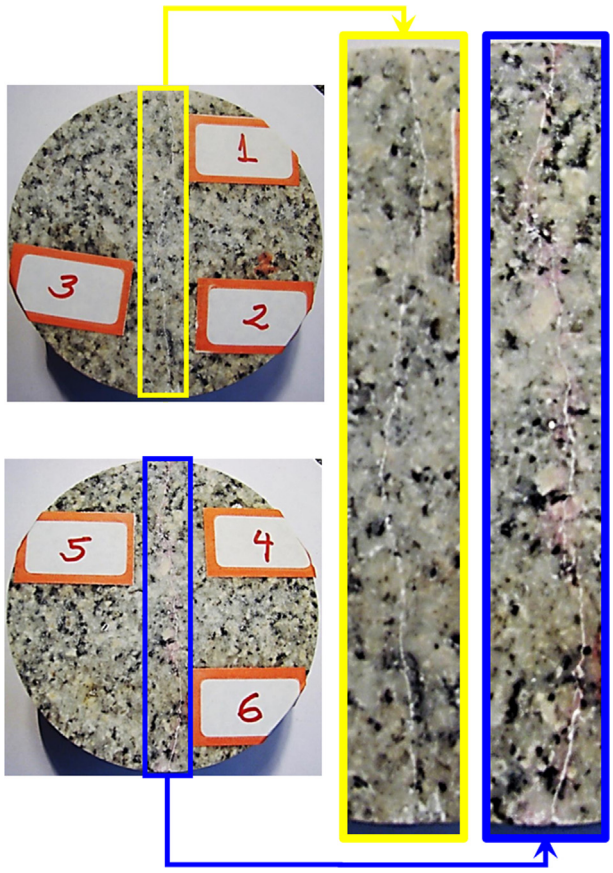

Fig. 3. Final cracking pattern on both faces of a typical specimen of monzogranite (identified as faces 123 and 456) and magnified view of the cracked area on face 123 (yellow rectangle) and face 456 (blue rectangle). The cracking pattern was similar on both faces of the specimen. (For interpretation of the references to color in this figure legend, the reader is referred to the web version of this article.)

The v_p values are calculated for each localized AE source by means of a process that involves the minimization of the adjustment error. In addition, each v_p value is associated with a region in the specimen volume defined along the trajectory between the AE source and each of the sensors that receive the signal emitted by this AE source. Therefore, the trend of the average v_p values, associated to each AE source allows the analysis of the distribution and evolution of damage, strength and stiffness inside the volume of the specimen during the loading process. The integrity of such region changes with the loading process. Therefore, v_p values change along the process, even for data coming from the same zone. Also, since v_p values obtained with CLAPWaVe for each AE source are calculated by using indirect measurements (AE signals), some dispersion in the distribution of the v_p values is expected. However, the expected dispersion in the v_p values does not hinder the trend of such data. For that reason, analyses of v_p values representative of the different zones at different loading stages, shown in Fig. 4e, g, i and k, are performed considering the trend of a moving average and not every single value. By using a moving average (as adopted by Aggelis, [37]), instead of every single value, the trend of v_p for each of the four zones of damage is better represented. Since the number of AE sources localized at each test is different, the length of the window is defined as 1% of total number of AE sources localized during the entire test. Such length is considered for analyses shown in Figs. 5 and 7.

For each of the four damaged zones the percentage of the total of AE sources localized during the entire test was recorded. As expected, the highest accumulation of AE sources was localized at the core zone. Over half of the AE sources localized during the test come from the internal core zone (54.6%). The contact zone showed the second highest accumulation of damage, with over one fourth of AE sources localized there (28.4%). The external core zone accumulated 15.3% of the total of AE sources localized during the test. An almost negligible number of AE sources (1.6%) were localized at the boundary zone. Despite small variation in percentages, the same trend was observed in all the diametral compression tests performed in monzogranite.

Fig. 4e shows that the AE sources are first localized at the contact zone. The values of v_p associated with the first AE sources are close to that of the intact material, but as the load increases, v_p also increases, showing the effect of confinement induced by the loading platens in the specimen. As the load increases, so does the damage at this contact zone (see Images 3 to 7 of Figs. 2 and 4e and f); therefore, the v_p value stabilizes instead of increasing through the end of the test.

Fig. 4g and h suggest the generation of a damaged central core, with the lowest v_p values of the specimen (much lower than that of the intact condition), and the highest levels of E_A release. As expected for this type of test, the central core zone shows the main concentration of damage (approximately 55% of the AE sources localized throughout the test) and the highest stiffness decrease.

In the external core zone (Fig. 4i), the associated v_p values oscillate around the v_p of the intact material, even though

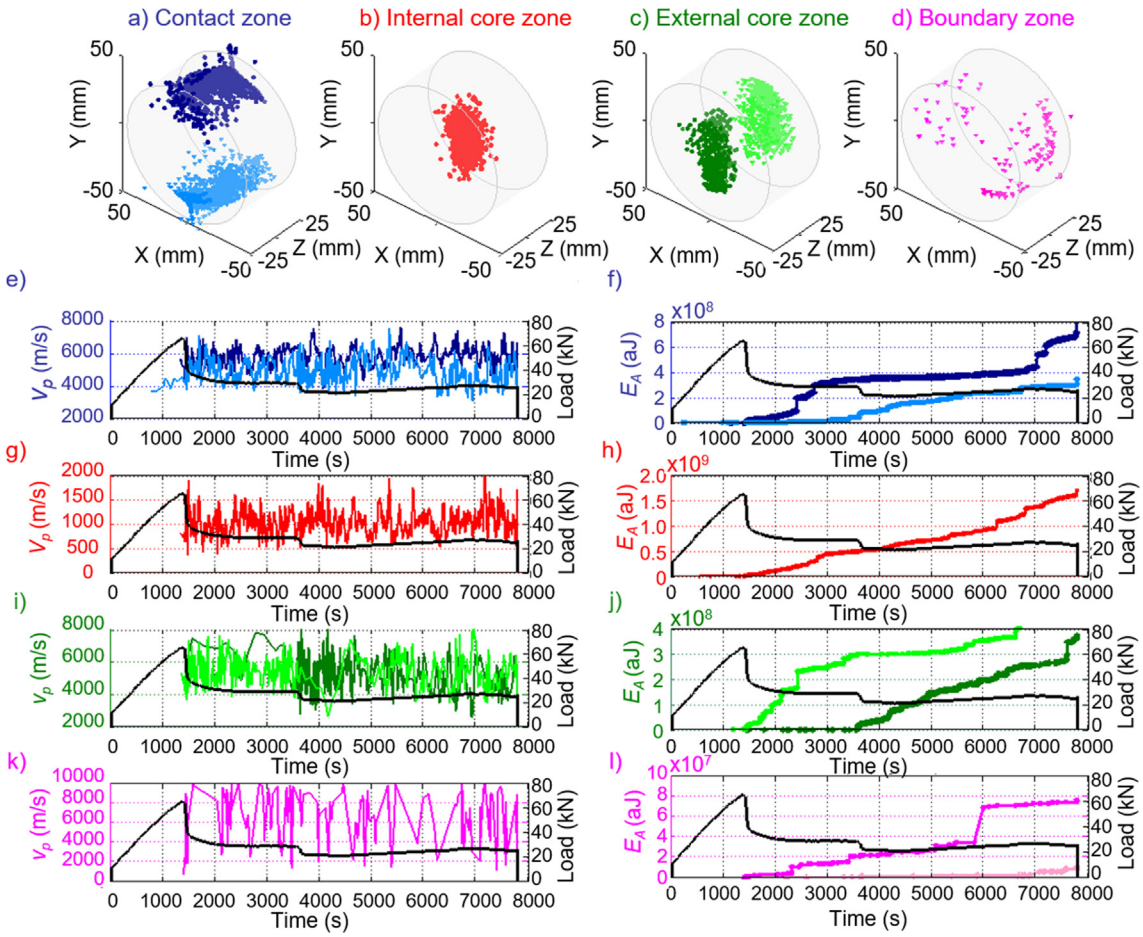

Fig. 4. Distribution of damage obtained by application of CLAPWaVe to a monzogranite specimen subjected to diametral compression test. Identified zones of damage (a to d), distribution of v_p and E_A for contact zone (e and f), central core (g and h), external core (i and j) and boundary zone (k and l).

microcracking progresses in this zone (high levels of E_A in Fig. 4j). This behavior is explained by considering that the waves generated in the external core zone must travel through highly damaged zones and other almost undamaged zones to reach the sensors.

The natural microscopic heterogeneity of the specimens explains the slightly asymmetrical distribution of damages on the faces of the specimen (E_A in Fig. 4f), and at its top and bottom (E_A in Fig. 4j).

The boundary zone (Fig. 4d) is a region with secondary microscopic cracking, generated as a result of the main damage process developed through the failure surface. After the failure surface has been created, following the loading axis of the specimen, the bending of its two halves may induce tension at the external borders. Fig. 4 shows scarce AE sources localized at this boundary zone (1.6%). The secondary microcracking is consistent with the existence of AE sources in this zone only at later stages of the test (after damage has progressed through the other three zones), and with the low level of E_A associated to them (100 times lower than those of the internal core, and 10 times lower than those of the external core or contact region). The low number of AE sources in this zone, and the influence of the other three zones on the trajectory of waves from the source to the sensors do not allow the visualization of a clear pattern of v_p values.

4.2. Typical behavior in marble under diametral compression tests

Similar to Fig. 2, Fig. 5 shows the spatial distribution of AE sources and v_p values associated to each AE source, during the test performed, in a marble specimen. The formatting for this figure is the same as in Fig. 2.

Image 1 of Fig. 5 shows AE sources localized at the central zone of the specimen volume (yellow and some green dots). Such AE sources accumulated at the center of the specimen are associated with v_p values lower than that of the intact material (4355 m/s), and lower than any other zone of the specimen. The v_p values associated to the AE sources localized at the center of the specimen and their higher levels of E_A released (see Fig. 7h) suggest that, they are associated with initiation and propagation of microcracking. Different from monzogranite, such pattern is observed from control point 1 in marble specimens, which suggests that the cracking process in marble initiates earlier than in monzogranite. The number of AE sources localized at the central zone of the specimen increases and they spread along the loading axis, as in monzogranite. The AE sources localized at the central zone of the marble specimen (Images 1 to 7 of Fig. 5) generate a central damaged core zone similar but more pronounced than that observed in Images 2 to 7 of Fig. 2 for monzogranite. Thus, the distribution of AE sources obtained with CLAPWaVe shows that, for marble specimens (Fig. 5), the failure surface has been already defined at the peak load, different from monzogranite specimens (Fig. 2).

Images 7 of Fig. 5 (planes XY and YZ) show the cracking pattern at the end of the test. Like the monzogranite specimens, a clear damaged core zone is observed in marble. Image 7 (plane YZ) clearly shows such region. The pattern of damage observed at the core zone of the specimen is consistent with the region of maximum tensile stress, resulting from the theoretical analyses of

diametral compression tests in isotropic and homogeneous materials [33,34,38].

In addition to the AE sources localized at the central region of the specimen, at control point 1 of Fig. 5, AE sources localized at the region of contact between the specimen and the loading platens are observed. From control point 1 to 3 (peak load) of Fig. 5, most of the AE sources localized at this contact region show v_p values lower than that of the intact material (4355 m/s). From control point 4 onwards, most of the AE sources localized at that region exhibit v_p values higher or similar to that of the intact material, as observed in the monzogranite.

The pattern of v_p of AE sources localized at the contact zone in images 1 to 7 of Fig. 5 shows that the three effects explained in section 4.1 for monzogranite are also observed in marble: 1) the load transfer between the specimen and the loading platens; 2) confinement induced by the loading platens to the specimen at the vicinity of the contact zone; 3) local rupture of the less confined region around the contact zone at later stages of the test. Until control point 3 (images 1 to 3 of Fig. 5), AE sources localized at this contact region mainly reflect the first effect. At control point 4 (Image 4 of Fig. 5), a combination of the first and the second effects is observed. From control point 5 onwards, effect 3 dominates. The lateral view (YZ plane) of the specimen at the end of the test (Image 7 of Fig. 5) shows accumulation of AE sources with associated low v_p values (yellow dots) right above the edge of the specimen, close to the region of Z = 25 mm and Y = 50 mm. The trend of the v_p values of such AE sources and their location suggest that they are mainly associated with effect 3. As expected, AE sources associated with effect 3 begin to accumulate from control points 4 or 5, when the general failure surface has been defined inside of the specimen. Such effect is observed earlier in marble, as a result of the earlier process of microcrack propagation in this rock, in comparison with the monzogranite.

Fig. 6 shows the final cracked specimen. The faces of the specimen are identified as explained in Fig. 3. The formatting is the same as in Fig. 3. To improve the visualization of the damaged area in the rock specimen, the color of the chalk dust was changed to pink to obtain a better contrast between the cracked and intact areas.

Fig. 6 shows that in this specimen, the cracking pattern was more concentrated in one of the faces (face 456). As the distributions of AE sources obtained with CLAPWaVe (Fig. 5) represent the cracking pattern in the rock specimen, the comparison between Figs. 5 and 6 show that the cracking pattern obtained with CLAPWaVe (Fig. 5) is consistent with the real damaged specimen at the end of the test (Fig. 6). Both the real damaged specimen and the cracking pattern obtained with CLAPWaVe show main concentration of microcracking at the same face. During the test, a centered and vertical crack only appeared on one of the faces of the specimen (face 456). Such non-homogeneous distribution of damage on both faces of the specimen is related to the natural heterogeneity of rock specimens.

Fig. 7 shows that the same four zones of damage accumulation were identified for the marble, as for monzogranite: contact region (blue sources, Fig. 7a), internal core (red sources, Fig. 7b), external core (green sources, Fig. 7c) and boundary zone (pink sources, Fig. 7d). The figure format is the same as for Fig. 4.

The percentage of AE sources localized at each of the four damaged zones was recorded. The highest accumulation of AE sources was localized at the internal core zone of the marble specimen, as shown for monzogranite. However, in marble specimens, a higher proportion of AE sources was localized at the internal core during all the tests (63.3% in marble versus 54.6% in monzogranite). The almost monomineralic structure of the marble, the presence of cleavage planes in their calcite crystals and the higher number of natural microcracks at its intact condition may explain the higher

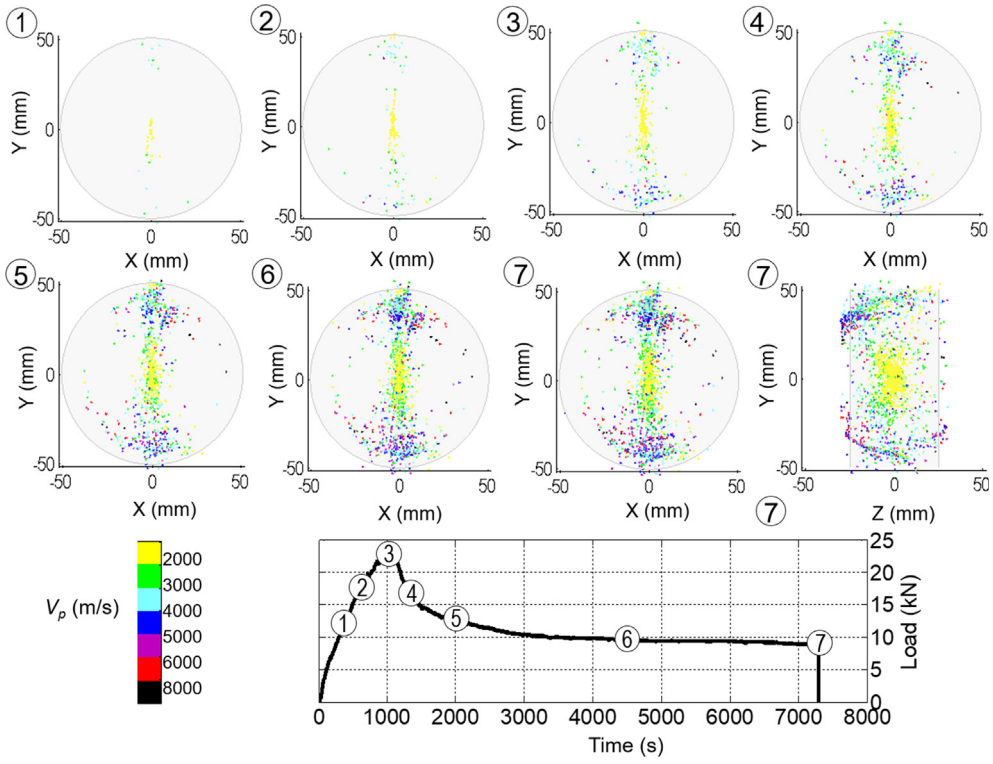

Fig. 5. Typical spatial distribution of AE sources and average v_p values at different stages of loading during monotonic displacement diametral compression test on a marble specimen (results obtained by application of CLAPWaVe).

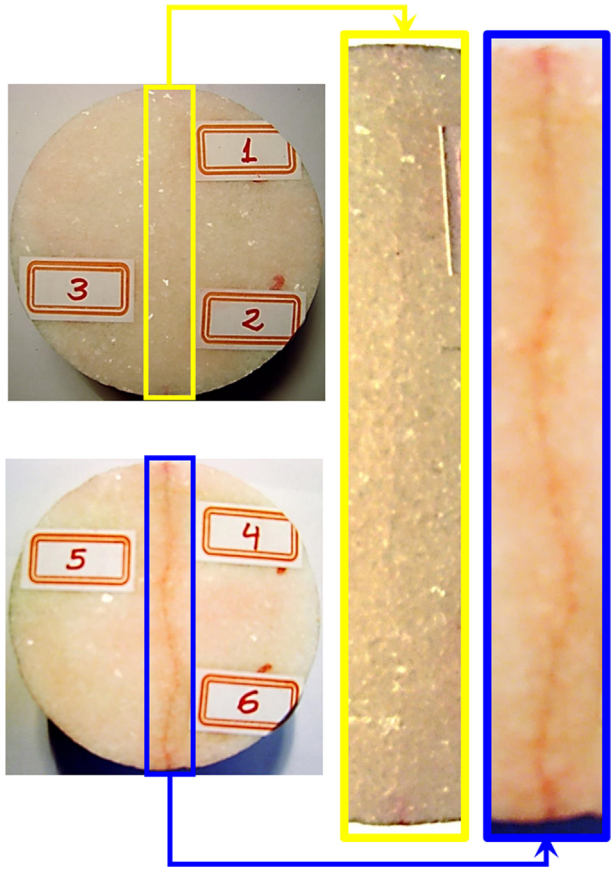

Fig. 6. Final cracking pattern on both faces of a typical specimen of marble (identified as faces 123 and 456) and magnified view of the cracked area on face 123 (yellow rectangle) and face 456 (blue rectangle). (For interpretation of the references to color in this figure legend, the reader is referred to the web version of this article.)

concentration of damage at the central core in this rock specimen, when compared with the monzogranite specimens. The latter are characterized by a polymineralic and imbricated structure without weakness planes for microcrack propagation, with a low number of natural microcracks. Similar to monzogranite, the contact zone showed the second highest accumulation of damage in marble, with 29.6% of the total of AE sources localized there (versus 28.4% for monzogranite). The external core zone accumulated 6.0% of the total of AE sources localized during the test, which is lower than in monzogranite (15.3%).

The sum of the percentages of AE sources localized in the internal and external core is 69.3% and for marble and 69.9% for monzogranite. Thus, both rocks show that the main accumulation of damage is located at the central part of the specimen, as expected for this type of test. However, in marble specimens, such damage was concentrated mainly in the core (central core zone), while monzogranite specimens showed higher proportion of damage distributed at the external core zone. Because the crystalline structure of monzogranite is more resistant to microcrack propagation, the less confined zone (external core zone) should concentrate a higher proportion of damage, which is consistent with the observed pattern. Also, such pattern is consistent with the progressive development of damage in monzogranite. Similar to monzogranite, an almost negligible number of AE sources (1.0% in marble and 1.6% in monzogranite) is localized at the boundary zone.

Fig. 7e shows that, during the earlier stages of microcracking (before and around control point 1 defined in Fig. 5), the v_p values associated with the AE sources localized at the contact zone are lower than that of the intact material (4355 m/s), because of the effect 1 explained in section 4.1. As the load increases, v_p also increases, showing the effect of confinement induced by the loading platens in the specimen (effect 2 explained in the analysis of Fig. 5). As the load increases, the increasing damage at the contact zone (Images 3 to 7 of Figs. 5 and 7e and f) results in v_p values with a decreasing trend through the end of the test. The earlier initiation and propagation of microcracks in marble specimens, and the earlier definition of the failure surface along the loading axis, explain the pronounced decreasing trend in v_p values at the post peak stages (in comparison with monzogranite specimens as shown in Fig. 4e).

Fig. 7j shows that energy release occurs essentially at one of the faces of the specimen (light green line, plane XY for z = -10 to −25 mm in Fig. 7c), which is consistent with the observed cracking pattern obtained with CLAPWaVe in Image 7 of Fig. 5, and with the final cracked specimen in Fig. 6 (face 456 is associated to AE sources in light green in Fig. 7c). Because there is more damage concentrated on one of the faces of the specimen, lower v_p values are expected at that face.

Comparison of Fig. 4f, h, j and l with Fig. 7f, h, j and l shows that the levels of E_A at each of the four zones are lower in marble (approximately 100 times lower). The lower levels of E_A are consistent with materials with the pre-existing cleavage planes.

Further research is still needed to determine the main reasons for the large variation of P-wave velocity observed in both type of rocks. The possible causes are: i) nonlinearity of the wave propagation process leading to the dependence of v_p on the E_A level; ii) velocity tends to be lower in a zone subjected to the tensile stresses due to microcrack opening, and higher in the compressed zones; iii) once a crack opens in a tensioned zone, tensile stresses are released, and the velocity may increase again.

Complementary analyses performed by clustering the AE sources based on their levels of absolute energy E_A and cited in section 4.1 enables an improved visualization of the cracking pattern in both rocks during all the test [1]. Although the patterns of the regions of damage accumulation are similar for both types of rocks (central core, external core, contact and boundary), the process of microcracks propagation at each zone is different for marble and monzogranite. Such conclusions are not contradictory. The marble and monzogranite specimens subjected to diametral compression tests exhibited different stages for microcrack initiation and progression of damage during the test. However, the same zones of damage accumulation are observed in both types of rocks. The polymineralic and imbricated internal structure of the monzogranite, the random distribution of minerals and the existence of few natural microcracks, do not leave clearly predefined paths for growing microcracks, which explains the difficulty in crack propagation through the rock specimen [16]. As a result, the crack propagation process is brittle, explosive, localized and followed by higher levels of E_A release. In contrast, in the monomineralic, non-imbricated structure of marble, the existence of three perfect cleavage planes in calcite crystals and the existence of many natural microcracks enhance crack propagation. Thus, when cracks propagate in marble, the process is slow, steady and followed by lower levels of E_A release. Despite the microscopic heterogeneity of the monzogranite structure and the presence of many naturally oriented microcracks in marble, both rocks exhibit macroscopic isotropy. Such aspect may be associated with the same loading conditions and the homogeneity of the macroscopic structure of both rocks. This suggests that the features of each rock influence the internal process of generation and propagation of damage, while the general pattern for regions of microcrack accumulation is mainly defined by the features of load transfer to the specimen.

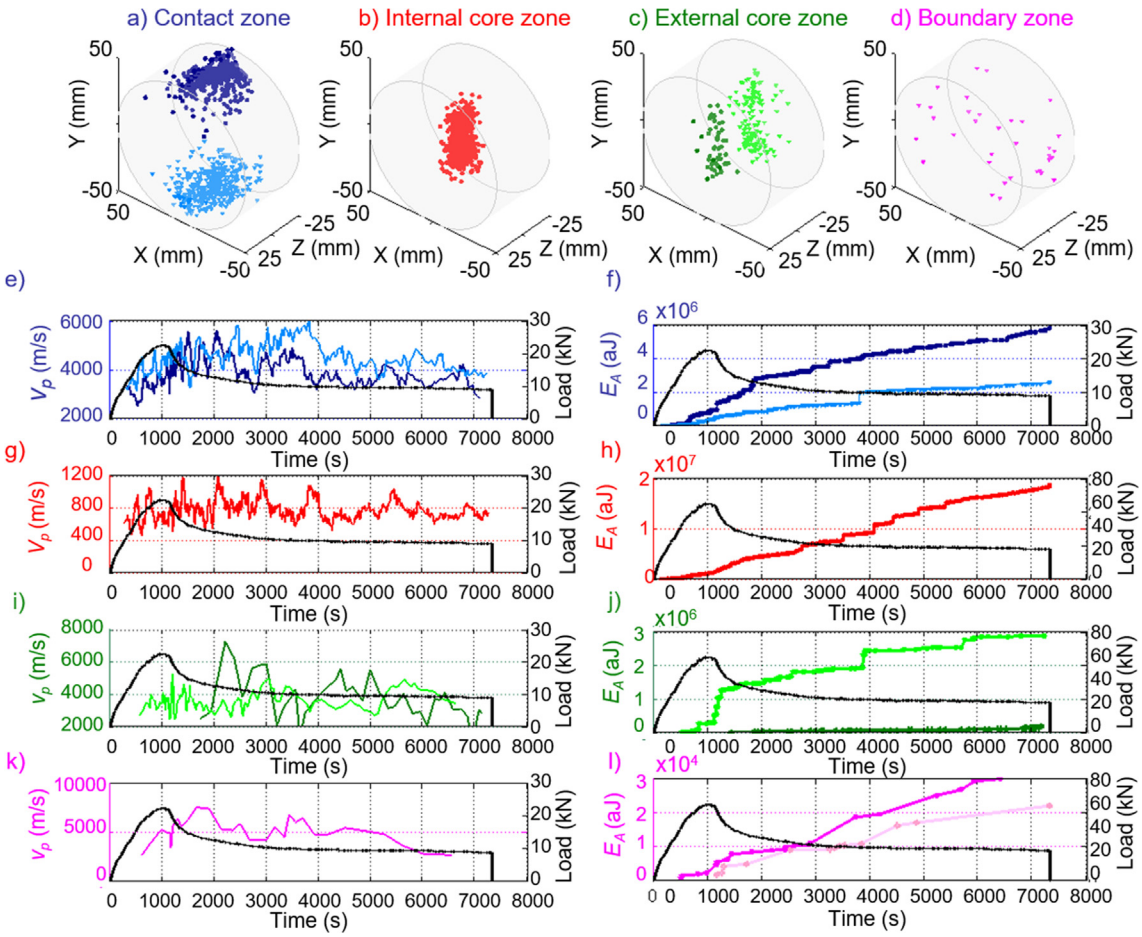

Fig. 7. Distribution of damage obtained by application of CLAPWaVe to a marble specimen subjected to diametral compression test. Identified zones of damage (a to d) and distribution of v_p and E_A for contact zone (e and f), central core (g and h), external core (i and j) and boundary zone (k and l).

5. Conclusions

An improved algorithm for localization of AE sources with v_p calculation and an enhanced methodology for the determination of P-wave onset time, called CLAPWaVe, is applied here to assess the distribution of damage within two different types of rock specimens subjected to diametral compression tests.

The determination of the average v_p values associated with each localized AE source provided important information related to the distribution and evolution of damage and stiffness variability, within the volume of the specimens, during the loading process. The complementary analyses of the pattern of AE sources and their associated v_p values and E_A showed a non-homogeneous distribution of damage, changing the characteristics of the specimen in comparison with its initial intact condition. Therefore, the use of a unique value for v_p equal to that of the intact material to localize all AE sources throughout the test is not representative of the real condition of the specimen, and may lead to unrealistic analyses.

Declaration of Competing Interest

The authors declare that they have no known competing financial interests or personal relationships that could have appeared to influence the work reported in this paper.

Acknowledgments

Financial support for the acquisition of the acoustic emission equipment was provided by FAPESP, the research funding agency for the State of São Paulo, Brazil (process No. 05/57250-2). The scholarship for the doctoral research of the first author was provided by CONICYT, the national research council of Chile (document No. 72120096).

References

[1] P. Rodríguez, Analysis of Microcracking in Rocks in Diametral Compression Tests Ph.D. dissertation, University of São Paulo, São Carlos, Brazil, 2015.
[2] J.F. Labuz, S. Cattaneo, L.H. Chen, Acoustic emission at failure in quasi-brittle materials, Constr. Build. Mater. 15 (5) (2001) 225–233, https://doi.org/10.1016/S0950-0618(00)00072-6.
[3] S.H. Chang, C.I. Lee, Estimation of cracking and damage mechanisms in rock under triaxial compression by moment tensor analysis of acoustic emission, Int. J. Rock Mech. Min. Sci. 41 (7) (2004) 1069–1086, https://doi.org/10.1016/j.ijrmms.2004.04.006.
[4] S. Köppel, C. Grosse, Advanced acoustic emission techniques for failure analysis in concrete, WCNDT Proc. (2000).
[5] J. Xu, Z. Fu, Q. Han, G. Lacidogna, A. Carpinteri, Micro-cracking monitoring and fracture evaluation for crumb rubber concrete based on acoustic emission techniques, Struct. Health Monit. 17 (4) (2018) 946–958, https://doi.org/10.1177/1475921717730538.
[6] Q. Han, G. Yang, J. Xu, Z. Fu, G. Lacidogna, A. Carpinteri, Acoustic emission data analyses based on crumb rubber concrete beam bending tests, Eng. Fract. Mech. 210 (2019) 189–202, https://doi.org/10.1016/j.engfracmech.2018.05.016.
[7] Q. Han, G. Yang, J. Xu, Experimental study on the relationship between acoustic emission energy and fracture energy of crumb rubber concrete, Struct. Control Health Monit. 25 (10) (2018), https://doi.org/10.1002/stc.2240 e2240.
[8] M. Ohtsu, T. Okamoto, S. Yuyama, Acoustic emission for cracking mechanisms in concrete, ACI Struct. J. 95 (1998) 87–95.
[9] A. Carpinteri, G. Lacidogna, G. Niccolini, Critical behaviour in concrete structures and damage localization by acoustic emission, Key Eng. Mater. 312 (2006) 305–310, https://doi.org/10.4028/www.scientific.net/KEM.312.305.

[10] J. Xu, S. Shu, Q. Han, C. Liu, Experimental research on bond behavior of reinforced recycled aggregate concrete based on the acoustic emission technique, Const. Build. Mater. 191 (2018) 1230–1241, https://doi.org/10.1016/j.conbuildmat.2018.10.054.
[11] N. Iverson, C. Kao, J.F. Labuz, Clustering analysis of AE in rock, J. Acoust. Emiss. 25 (2007) 364–372.
[12] L. Jian-po, L. Yuan-hui, X. Shi-da, X. Shuai, J. Chang-yu, Cracking mechanisms in granite rocks subjected to uniaxial compression by moment tensor analysis of acoustic emission, Theor. Appl. Fract. Mech. 75 (2015) 151–159, https://doi.org/10.1016/j.tafmec.2014.12.006.
[13] Q. Han, J. Xu, A. Carpinteri, G. Lacidogna, Localization of acoustic emission sources in structural health monitoring of masonry bridge, Struct. Control Hlt. 22 (2) (2015) 314–329, https://doi.org/10.1002/stc.1675.
[14] P. Rodríguez, P. Arab, T.B. Celestino, Characterization of rock cracking patterns in diametral compression tests by acoustic emission and petrographic analysis, Int. J. Rock Mech. Min. Sci. 83 (2016) 73–85, https://doi.org/10.1016/j.ijrmms.2015.12.017.
[15] F. Ciampa, M. Meo, A New algorithm for acoustic emission localization and flexural group velocity, Compos. Part A-Appl. S. 41 (12) (2010) 1777–1786, https://doi.org/10.1016/j.compositesa.2010.08.013.
[16] P. Rodríguez, T.B. Celestino, Application of acoustic emission monitoring and signal analysis to the qualitative and quantitative characterization of the fracturing process in rocks, Eng. Fract. Mech. 210 (2019) 54–69, https://doi.org/10.1016/j.engfracmech.2018.06.027.
[17] V. Salinas, Y. Vargas, J. Ruzzante, L. Gaete, Localization algorithm for acoustic emission, Phys. Procedia 3 (1) (2010) 863–871.
[18] E. Aker, D. Kühn, V. Vavryčuk, M. Soldal, V. Oye, Experimental investigation of acoustic emissions and their moment tensors in rock during failure, Int. J. Rock Mech. Min. Sci. 70 (2014) 286–295, https://doi.org/10.1016/j.ijrmms.2014.05.003.
[19] X. Li, L. Dong, An Efficient closed-form solution for acoustic emission source location in three-dimensional structures, AIP Adv. 4 (2) (2014), https://doi.org/10.1063/1.4866170 027110.
[20] A. Carpinteri, G. Lacidogna, G. Niccolini, S. Puzzi, Morphological fractal dimension versus power-law exponent in the scaling of damaged media, Int. J. Damage Mech. 18 (2009) 259–282, https://doi.org/10.1177/1056789508098700.
[21] I. Iturrioz, G. Lacidogna, A. Carpinteri, Acoustic emission detection in concrete specimens: experimental analysis and lattice model simulations, Int. J. Damage Mech. 2 (2014) 327–358, https://doi.org/10.1177/1056789513494232.
[22] G. Manthei, Application of the cluster analysis and time statistic of acoustic emission events from tensile test of acylindrical rock salt specimen, Eng. Fract. Mech. 210 (2019) 84–94, https://doi.org/10.1016/j.engfracmech.2018.05.039.
[23] T.B. Celestino, A. Bortolucci, C. Nobrega, Determination of rock fracture toughness under creep and fatigue, in: Proceedings of the US Symposium on Rock Mechanics, Reno, New York, 5–7 June, 1995, pp. 147–152.
[24] T.B. Celestino, R. Piltner, P.J.M. Monteiro, C.P. Ostertag, Fracture mechanics of marble using a splitting tension test, J. Mater. Civ. Eng. 13 (6) (2001) 407–411.
[25] Mistras Group Inc., AEwin™ Software User's Manual. Rev. 3, Products & Systems Division, Princeton Junction, New Jersey, USA, 2009.
[26] A.F. Prugger, D.J. Gendzwill, Microearthquake location: a nonlinear approach that makes use of a simplex stepping procedure, Bull. Seismol. Soc. Am. 78 (2) (1988) 799–815.
[27] W.H. Press, B.P. Flannery, S.A. Teukolsky, W.T. Vetterling, Numerical Recipes in C: The Art of Scientific Computing, Cambridge University, 1992.
[28] J.H. Kurz, C.U. Grosse, H.W. Reinhardt, Strategies for reliable automatic onset item picking of acoustic emissions and of ultrasound signals in concrete, Ultrasonics 43 (2005) 538–546, https://doi.org/10.1016/j.ultras.2004.12.005.
[29] A. Carpinteri, J. Xu, G. Lacidogna, A. Manuello, Reliable onset time determination and source, Cem. Concr. Compos. 34 (4) (2012) 529–537, https://doi.org/10.1016/j.cemconcomp.2011.11.013.
[30] F. Carvalho, Characterizing Brittle Failure through Quantitative Acoustic Emission Ph.D. Thesis, University of Minnesota, USA, 1999.
[31] M.J. Eaton, R. Pullin, K.M. Holford, Towards improved damage location using acoustic emission, Proc. Mech. Eng. Part C: J. Mech. Eng. 226 (9) (2012) 2141–2153, https://doi.org/10.1177/0954406212449582.
[32] H.R. Hardy, Acoustic Emission/Microseismic Activity: Volume 1: Principles, Techniques and Geotechnical Applications, CRC Press, 2005.
[33] K.T. Chau, X.X. Wei, A three-dimensional analytic solution for the Brazilian test, in: *2nd Asian Rock Mechanics Symposium*, Beijing, China, 11–14 September, 2001, pp. 141–144.
[34] G. Hondros, The Evaluation of Poisson's ratio and the modulus of materials of a low tensile resistance by the Brazilian (indirect tensile) test with particular reference to concrete, Aust. J. Appl. Sci. 10 (3) (1959) 243–268.
[35] D. Li, L.N.Y. Wong, The Brazilian disc test for rock mechanics applications: review and new insights, Rock Mech. Rock Eng. 46 (2) (2013) 269–287, https://doi.org/10.1007/s00603-012-0257-7.
[36] H. Hertz, Gesammelte Werke (Collected Works), Leipzig. [S.l.:s.n.], 1895.
[37] D.G. Aggelis, Classification of cracking mode in concrete by acoustic emission parameters, Mech. Res. Commun. 38 (2) (2011) 153–157, https://doi.org/10.1016/j.mechrescom.2011.03.007.
[38] X.X. Wei, K.T. Chau, Three dimensional analytical solution for finite circular cylinders subjected to indirect tensile test, Int. J. Solids Struct. 50 (14–15) (2013) 2395–2406.